

## Gas Separation

International Edition: DOI: 10.1002/anie.202000323  
German Edition: DOI: 10.1002/ange.202000323Mixed Metal–Organic Framework with Multiple Binding Sites for Efficient C<sub>2</sub>H<sub>2</sub>/CO<sub>2</sub> Separation

Junkuo Gao,\* Xuefeng Qian, Rui-Biao Lin,\* Rajamani Krishna, Hui Wu, Wei Zhou,\* and Banglin Chen\*

**Abstract:** The separation of C<sub>2</sub>H<sub>2</sub>/CO<sub>2</sub> is particularly challenging owing to their similarities in physical properties and molecular sizes. Reported here is a mixed metal–organic framework (M'MOF), [Fe(py<sub>2</sub>)Ni(CN)<sub>4</sub>] (**FeNi-M'MOF**, py<sub>2</sub> = pyrazine), with multiple functional sites and compact one-dimensional channels of about 4.0 Å for C<sub>2</sub>H<sub>2</sub>/CO<sub>2</sub> separation. This MOF shows not only a remarkable volumetric C<sub>2</sub>H<sub>2</sub> uptake of 133 cm<sup>3</sup> cm<sup>-3</sup>, but also an excellent C<sub>2</sub>H<sub>2</sub>/CO<sub>2</sub> selectivity of 24 under ambient conditions, resulting in the second highest C<sub>2</sub>H<sub>2</sub>-capture amount of 4.54 mol L<sup>-1</sup>, thus outperforming most previous benchmark materials. The separation performance of this material is driven by π–π stacking and multiple intermolecular interactions between C<sub>2</sub>H<sub>2</sub> molecules and the binding sites of **FeNi-M'MOF**. This material can be facilely synthesized at room temperature and is water stable, highlighting **FeNi-M'MOF** as a promising material for C<sub>2</sub>H<sub>2</sub>/CO<sub>2</sub> separation.

**M**etal–organic frameworks (MOFs) have emerged as very promising porous materials for adsorptive gas separation because they integrate the merits of tunable pore sizes and functional pore surfaces that can realize not only a molecular sieving effect, but also preferential gas binding.<sup>[1]</sup> Many MOFs have been explored for simplifying various gas separation and purification schemes ranging from mature ones, such as carbon dioxide capture (CO<sub>2</sub>) from methane and nitrogen, to more challenging olefin/paraffin and alkyne/alkene separations.<sup>[2]</sup> For C<sub>2</sub>H<sub>2</sub> and CO<sub>2</sub> gas molecules, the similarities in

physical properties (differ in boiling point by ca. 3 % and ca. 6 K) and identical molecular shapes/sizes (3.3 × 3.3 × 5.7 Å<sup>3</sup> for C<sub>2</sub>H<sub>2</sub>, 3.2 × 3.3 × 5.4 Å<sup>3</sup> for CO<sub>2</sub>), with kinetic diameters of about 3.3 Å, make it very difficult and challenging to realize efficient porous materials for C<sub>2</sub>H<sub>2</sub>/CO<sub>2</sub> separation under ambient conditions.<sup>[3]</sup> A few ultra-microporous MOFs featuring bare oxygen or fluorine base sites have been developed to preferentially bind C<sub>2</sub>H<sub>2</sub> molecules through hydrogen-bonding interactions or bind CO<sub>2</sub> molecules through electrostatic interactions, showing high C<sub>2</sub>H<sub>2</sub>/CO<sub>2</sub> selectivity but low C<sub>2</sub>H<sub>2</sub> uptake.<sup>[4]</sup> Another approach is to incorporate strong adsorption binding sites, mainly open metal sites, into MOFs with large pore volumes to boost the uptake capacity of the preferred gas molecules.<sup>[5]</sup> **UTSA-74** represents a unique example with open metal centers having two accessible sites which can bind two C<sub>2</sub>H<sub>2</sub> molecules, but only one CO<sub>2</sub> molecule, differing from its isomer **MOF-74** which adsorbs similar amounts of C<sub>2</sub>H<sub>2</sub> and CO<sub>2</sub> under the same conditions.<sup>[5c]</sup> Though progress has been made over the past several years, the uptake capacity versus selectivity trade-off still poses a daunting challenge for addressing C<sub>2</sub>H<sub>2</sub>/CO<sub>2</sub> separation.<sup>[6]</sup>

The vast database of reported MOF structures enables comparative analyses to target potential candidates with dual functionalities, featuring moderate pore volumes and accessible functional sites, to realize both high gas uptake and separation selectivities. Among plentiful ligands, cyanide is a short and highly basic ligand that is feasible to construct robust MOFs with modest pore aperture size, such as Prussian blue and Hofmann-type compounds.<sup>[7]</sup> For those MOFs with metalloligands, the open metal sites on ligands are accessible for gas molecules, whereas expected narrow pore structures originating from compact ligands enforce additional multiple intermolecular interactions to form, as demonstrated by a series of mixed metal–organic frameworks (M'MOFs).<sup>[8]</sup> In this regard, a Hofmann-type MOF [Fe(py<sub>2</sub>)Ni(CN)<sub>4</sub>] (**FeNi-M'MOF**, py<sub>2</sub> = pyrazine), discovered in 2001, showing open nickel sites and polarized surfaces as well as compact pore channels of about 4.0 Å, is particularly interesting.<sup>[9]</sup> The high density of functional sites and ultra-micropore would collaboratively enforce gas separation with high gas uptake and separation selectivities. Herein we investigate the mixed iron/nickel MOF **FeNi-M'MOF** for potential C<sub>2</sub>H<sub>2</sub>/CO<sub>2</sub> separation. In this MOF, C<sub>2</sub>H<sub>2</sub> molecules are found to preferentially bind the organic moieties and open Ni sites through π–π stacking and multiple intermolecular interactions, respectively, whereas CO<sub>2</sub> molecules mainly distribute on the open Ni sites through relatively weak interactions. In this context, **FeNi-M'MOF** shows a very high C<sub>2</sub>H<sub>2</sub>/CO<sub>2</sub> selectivity of 24 that is superior to the previous top-perform-

[\*] Prof. J. Gao, X. Qian

Institute of Functional Porous Materials, The Key Laboratory of Advanced Textile Materials and Manufacturing Technology of Ministry of Education, School of Materials Science and Engineering, Zhejiang Sci-Tech University, Hangzhou 310018 (China)  
E-mail: jkgao@zstu.edu.cn

Prof. J. Gao, Dr. R.-B. Lin, Prof. B. Chen

Department of Chemistry, University of Texas at San Antonio  
One UTSA Circle, San Antonio, TX 78249-0698 (USA)  
E-mail: ruibiao.lin@utsa.edu  
banglin.chen@utsa.edu

Dr. R. Krishna

Van't Hoff Institute of Molecular Sciences, University of Amsterdam  
Science Park 904, 1098 XH Amsterdam (The Netherlands)

Dr. H. Wu, Dr. W. Zhou

NIST Center for Neutron Research, National Institute of Standards and Technology, Gaithersburg, MD 20899-6102 (USA)  
E-mail: wzhou@nist.govSupporting information and the ORCID identification number(s) for the author(s) of this article can be found under:  
<https://doi.org/10.1002/anie.202000323>.

ing MOFs while retaining a remarkable  $C_2H_2$  uptake capacity of  $133\text{ cm}^3\text{ cm}^{-3}$ , and thus an excellent  $C_2H_2$ -capture capacity of  $4.54\text{ mol L}^{-1}$  at 298 K and 1 bar for 50:50  $C_2H_2/CO_2$  separation, which is close to that of the benchmark UTSA-74 and exceeds that of other out-performing MOFs.<sup>[5c]</sup>

**FeNi-M'MOF** is a pillared-layer M'MOF, in which the  $Fe[Ni(CN)_4]$  layer is connected by the pyz pillars. The Ni atoms show square-planar coordination geometry while Fe atoms are octahedrally coordinated. The Ni atoms are coordinated by carbon atoms of four different cyan groups, whereas the Fe atoms are fully coordinated by nitrogen atoms from four different cyan groups and two pyz linkers.  $Fe[Ni(CN)_4]$  layers are then connected by pyz linkers into a three-dimensional network with one-dimensional channels of about  $4.15 \times 4.27$  or  $3.94 \times 4.58\text{ \AA}^2$ . The open metal site density of **FeNi-M'MOF** is about  $9.2\text{ mmol cm}^{-3}$ , which is higher than that of most MOFs, as shown in Table S2 (see the Supporting Information).

**FeNi-M'MOF** was synthesized at room temperature in water and methanol (Figure 1).<sup>[10]</sup> By adding the solution of  $K_2[Ni(CN)_4]$  into the mixed methanol and water solution of  $Fe^{2+}$  and pyz, the **FeNi-M'MOF** microcrystalline powders were obtained after stirring for 30 minutes. The powder X-ray diffraction (PXRD) of products indicated that those products have a good crystallinity and match well with the simulated XRD pattern, indicating the purity of **FeNi-M'MOF**. The resultant **FeNi-M'MOF** was further validated by elemental analysis (EA), thermogravimetry analysis (TGA), energy dispersive spectroscopy (EDS), and X-ray photoelectron spectroscopy (XPS) analysis (see the Supporting Information). This MOF also exhibits excellent water stability as shown in Figure S2. After soaking in water for 30 days, the crystallinity of **FeNi-M'MOF** is still retained. The TGA curve indicated that **FeNi-M'MOF** exhibits a considerable thermal stability up to  $200^\circ\text{C}$  (see Figure S4). The thermal stability of **FeNi-M'MOF** was also confirmed by variable-temperature PXRD (see Figure S5), indicating that **FeNi-M'MOF** can maintain its crystalline structure up to about  $200^\circ\text{C}$ . The fast and facile synthesis method, excellent water stability, and good thermal stability indicate **FeNi-M'MOF** is a promising separation material for scale-up synthesis.

The Brunauer-Emmett-Teller (BET) surface area

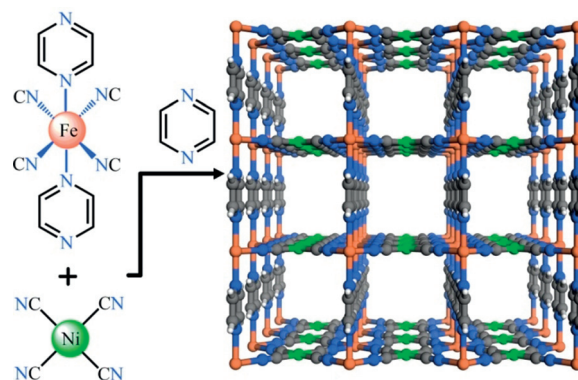


**Figure 1.** The crystal structure of **FeNi-M'MOF** viewed along the  $a/b$  axis. Fe, Ni, C, N, and H in **FeNi-M'MOF** are represented by orange, green, gray, blue, and white, respectively.

of **FeNi-M'MOF** was measured to be  $383\text{ m}^2\text{ g}^{-1}$  by an  $N_2$  sorption experiment at 77 K as shown in Figure 2a. The experimental total pore volume is about  $0.25\text{ cm}^3\text{ g}^{-1}$ , and slightly smaller than the theoretical one calculated from the crystal structure ( $0.30\text{ cm}^3\text{ g}^{-1}$ ), which can be attributed to the insufficient filling of  $N_2$  molecules in the ultramicroporous pore channels.

The  $C_2H_2$  and  $CO_2$  gas adsorption isotherms of **FeNi-M'MOF** were measured at both 273 and 298 K. As shown in Figure 2b, the volumetric  $C_2H_2$  uptake capacity of **FeNi-M'MOF** is  $133\text{ cm}^3\text{ cm}^{-3}$  ( $4.29\text{ mmol g}^{-1}$ ) at 1 bar and 298 K,

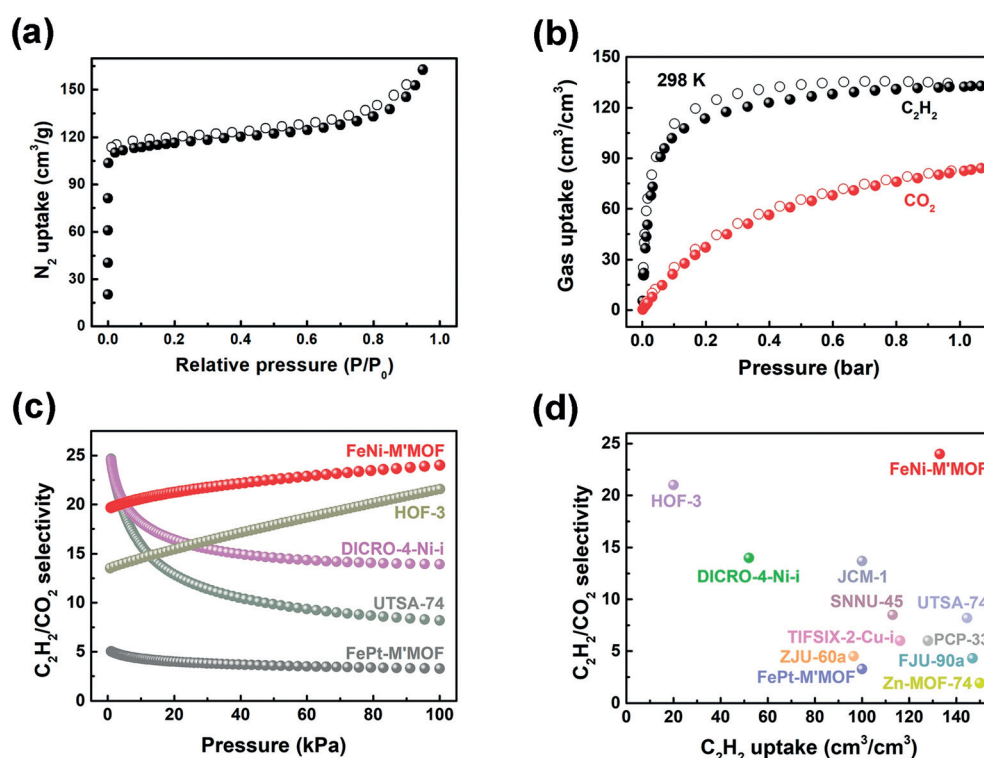


**Figure 2.** a)  $N_2$  sorption isotherms for **FeNi-M'MOF** at 77 K. b)  $C_2H_2$  and  $CO_2$  sorption isotherms for **FeNi-M'MOF** at 298 K. c) Comparison of IAST selectivities for equimolar  $C_2H_2/CO_2$  mixtures in **FeNi-M'MOF**, **FePt-M'MOF** and other materials in the range of 0–1 bar at 298 K. d) Comparison of  $C_2H_2/CO_2$  adsorption selectivity and volumetric  $C_2H_2$  uptake at 1 bar in **FeNi-M'MOF**, **FePt-M'MOF** and other porous materials.

which is higher than those of many other MOFs, such as **DICRO-4-Ni-i** ( $52 \text{ cm}^3 \text{ cm}^{-3}$ ),<sup>[4e]</sup> **ZJU-60a** ( $96 \text{ cm}^3 \text{ cm}^{-3}$ ),<sup>[11]</sup> **Cu[Ni(pdt)<sub>2</sub>]** ( $108 \text{ cm}^3 \text{ cm}^{-3}$ ),<sup>[6a]</sup> **SNNU-45** ( $113 \text{ cm}^3 \text{ cm}^{-3}$ ),<sup>[6b]</sup> **TIFSIX-2-Cu-i** ( $116 \text{ cm}^3 \text{ cm}^{-3}$ ),<sup>[4f]</sup> **PCP-33** ( $128 \text{ cm}^3 \text{ cm}^{-3}$ ),<sup>[12]</sup> and comparable to those of **UTSA-74** ( $144 \text{ cm}^3 \text{ cm}^{-3}$ ),<sup>[5c]</sup> **FJU-90a** ( $146 \text{ cm}^3 \text{ cm}^{-3}$ ),<sup>[6c]</sup> and **Zn-MOF-74** ( $150 \text{ cm}^3 \text{ cm}^{-3}$ ).<sup>[13]</sup> The  $\text{CO}_2$  uptake of **FeNi-M'MOF** is  $84 \text{ cm}^3 \text{ cm}^{-3}$  ( $2.72 \text{ mmol g}^{-1}$ ) at 1 bar and 298 K. At 1 bar and 273 K,  $\text{C}_2\text{H}_2$  and  $\text{CO}_2$  uptakes of **FeNi-M'MOF** are up to 145 and  $102 \text{ cm}^3 \text{ cm}^{-3}$  respectively, as shown in Figure S8. Interestingly, the Pt analogue  $[\text{Fe}(\text{pyz})\text{Pt}(\text{CN})_4]$  (**FePt-M'MOF**; see Figures S10–S12) shows much lower uptake capacities for  $\text{C}_2\text{H}_2$  and  $\text{CO}_2$  ( $100$  and  $105 \text{ cm}^3 \text{ cm}^{-3}$ , respectively), indicating the potential binding contribution of Ni sites in this type of MOF for  $\text{C}_2\text{H}_2$  molecules. To evaluate the separation performance of this material, ideal adsorbed solution theory (IAST) was employed to calculate the adsorption selectivity. As shown in Figure 2c, at 100 kPa and 298 K, the  $\text{C}_2\text{H}_2/\text{CO}_2$  (50:50) selectivity of **FeNi-M'MOF** is 24. The selectivity of **FeNi-M'MOF** is higher than those of most MOFs, such as **Zn-MOF-74** (1.92),<sup>[5c]</sup> **FJU-90a** (4.3),<sup>[6c]</sup> **UTSA-74a** (8.2),<sup>[5c]</sup> **JCM-1** (13.4),<sup>[4b]</sup> **DICRO-4-Ni-i** (13.9),<sup>[4e]</sup> and benchmark **HOF-3a** (21).<sup>[14]</sup> It should be noted that both the uptake capacity and separation selectivity can significantly affect the practical performance of an adsorbent. **HOF-3a** has a high selectivity, but the low uptake of  $\text{C}_2\text{H}_2$  reduced its separation performance. In contrast, **FeNi-M'MOF** can address such trade-offs between the adsorption capacity and selectivity as shown in Figure 2d. The high selectivity and high  $\text{C}_2\text{H}_2$  adsorption capacity of **FeNi-M'MOF** jointly reveal its useful separation potential for  $\text{C}_2\text{H}_2/\text{CO}_2$ .

Transient breakthrough simulations were conducted to demonstrate the  $\text{C}_2\text{H}_2/\text{CO}_2$  separation performance of **FeNi-M'MOF**. The simulations in Figure 3a demonstrate the **FeNi-M'MOF** is of potential use for this challenging separation of  $\text{C}_2\text{H}_2/\text{CO}_2$  mixtures. The  $\text{C}_2\text{H}_2/\text{CO}_2$  mixtures (50:50) were used as feeds to mimic the industrial process conditions. Pure  $\text{CO}_2$  first eluted through the bed, where the  $\text{CO}_2$  purity was 99.95 %, followed by the breakthrough of  $\text{C}_2\text{H}_2$  after a certain time,  $\tau_{\text{break}}$ , during which **FeNi-M'MOF** was saturated by  $\text{C}_2\text{H}_2$ . The  $\text{C}_2\text{H}_2$ -capture amount of **FeNi-M'MOF** is  $4.54 \text{ mol L}^{-1}$  based on the simulated column breakthrough, which is close to that of the benchmark **UTSA-74** ( $4.86 \text{ mol L}^{-1}$ )<sup>[5c]</sup> and higher than those of most out-perform-

ing MOFs, such as **Zn-MOF-74** ( $4.06 \text{ mol L}^{-1}$ ),<sup>[5c]</sup> **FJU-90a** ( $4.16 \text{ mol L}^{-1}$ ),<sup>[6c]</sup> and **PCP-33** ( $4.16 \text{ mol L}^{-1}$ ).<sup>[12]</sup> Accordingly, **FeNi-M'MOF** shows not only a high  $\text{C}_2\text{H}_2/\text{CO}_2$  selectivity and high  $\text{C}_2\text{H}_2$  uptake but also high  $\text{C}_2\text{H}_2$ -capture capability from gas mixtures, endowing this material with a useful  $\text{C}_2\text{H}_2/\text{CO}_2$  separation potential. Based on experimental breakthrough studies, we further evaluated the performance of **FeNi-M'MOF** in near practical separation processes for a  $\text{C}_2\text{H}_2/\text{CO}_2$  mixture (50:50 v/v) as shown in Figure 3b. Indeed, **FeNi-M'MOF** exhibits excellent  $\text{C}_2\text{H}_2/\text{CO}_2$  mixture separation performance at 298 K.  $\text{CO}_2$  was first eluted through the adsorption bed without any detectable  $\text{C}_2\text{H}_2$ , whereas the latter was retained in the MOF column for a remarkable period prior to saturate the MOF. The retention time of pure  $\text{CO}_2$  and  $\text{C}_2\text{H}_2$  for  $\text{C}_2\text{H}_2/\text{CO}_2$  (50:50 v/v) mixture on **FeNi-M'MOF** are up to 24 and 40 min, respectively. Accordingly, the captured  $\text{C}_2\text{H}_2$  was calculated to be  $4.10 \text{ mol L}^{-1}$  with a separation factor of 1.7.

The isosteric heat of adsorption ( $Q_{\text{st}}$ ) has been used to evaluate the strength of interaction between the adsorbent and the adsorbate, which is calculated (see Figure S13) from the adsorption isotherms at 273 and 298 K. The  $Q_{\text{st}}$  values are 27–32.8 and about  $24.5 \text{ kJ mol}^{-1}$  of **FeNi-M'MOF** for  $\text{C}_2\text{H}_2$  and  $\text{CO}_2$ , respectively. The  $Q_{\text{st}}$  value of  $\text{C}_2\text{H}_2$  in **FeNi-M'MOF** is lower than those of other MOFs such as **HKUST-1** ( $39 \text{ kJ mol}^{-1}$ ),<sup>[15]</sup> **FeMOF-74** ( $47.5 \text{ kJ mol}^{-1}$ ),<sup>[16]</sup> and **SIFSIX-2-Cu-i** ( $41.9 \text{ kJ mol}^{-1}$ ),<sup>[1e]</sup> and is comparable to that of **UTSA-74** ( $31 \text{ kJ mol}^{-1}$ ).<sup>[5c]</sup> These data indicate **FeNi-M'MOF** has a lower regeneration energy for  $\text{C}_2\text{H}_2$  production, which would be beneficial for practical applications.

To understand the separation performance of **FeNi-M'MOF**, the adsorption modes of  $\text{C}_2\text{H}_2$  in **FeNi-M'MOF** were established by DFT-D calculations (see Figure S14). The modeling structures indicated that there are two binding sites for  $\text{C}_2\text{H}_2$  in **FeNi-M'MOF**: Site I, located in the middle of two adjacent pyz rings, where  $\text{C}_2\text{H}_2$  was adsorbed through the  $\pi$ - $\pi$  interactions between  $\text{C}_2\text{H}_2$  and the pyz rings (see Figure S14a). The  $\text{C}_2\text{H}_2$  static binding energy in site I is up to  $41.4 \text{ kJ mol}^{-1}$ . Site II, located in the middle of two adjacent Ni open metal sites, where  $\text{C}_2\text{H}_2$  a molecule is adsorbed through the interactions between  $\text{C}\equiv\text{C}$  and Ni open metal sites and is perpendicular to  $c$  axis. The  $\text{C}_2\text{H}_2$  static binding energy in this site is  $29.9 \text{ kJ mol}^{-1}$ , which is smaller than that of site I (see Figure S14b).

Further visualization of these host-guest interactions was carried out through high-resolution neutron powder diffraction experiments. The crystal structure under low  $\text{C}_2\text{D}_2$  loading was measured first (Figure 4a). As expected,  $\text{C}_2\text{D}_2$  molecules preferentially distribute on site I.  $\text{C}_2\text{D}_2$  molecules were identified between the two pyz rings through  $\pi$ - $\pi$  stacking ( $3.552 \text{ \AA}$ ). The  $\text{C}_2\text{D}_2$  molecules show a titling angle of  $27.4^\circ$  from the [001] direction (crystallographic  $c$  axis; see Figure S15a). In addition, multiple intermolecular interactions were also observed between  $\text{C}_2\text{D}_2$  and **FeNi-M'MOF** ( $\text{D}^{\delta+}\cdots\text{N}^{\delta-}$ :  $2.977 \text{ \AA}$ ,  $\text{C}^{\delta-}\cdots\text{N}^{\delta-}$ :  $3.808 \text{ \AA}$ , Figure 4c; see Figure S15b). In contrast, the preferential  $\text{CO}_2$  binding site is located at the open Ni site (Figure 4b). The electronegative  $\text{O}^{\delta-}$  atoms of  $\text{CO}_2$  interact with the positive open-metal site  $\text{Ni}^{\delta+}$ . However, the distance across the channel is insufficient

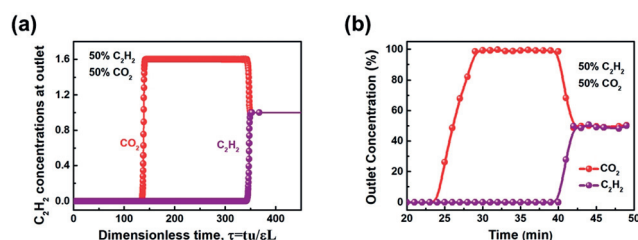


**Figure 3.** a) Transient breakthrough simulations for separation of equimolar  $\text{C}_2\text{H}_2/\text{CO}_2$  mixture using **FeNi-M'MOF** at 298 K, with a partial pressure of 50 kPa for each. b) Experiment breakthrough curves for equimolar  $\text{C}_2\text{H}_2/\text{CO}_2$  mixture in a packed column with **FeNi-M'MOF** at 298 K and 1 bar.

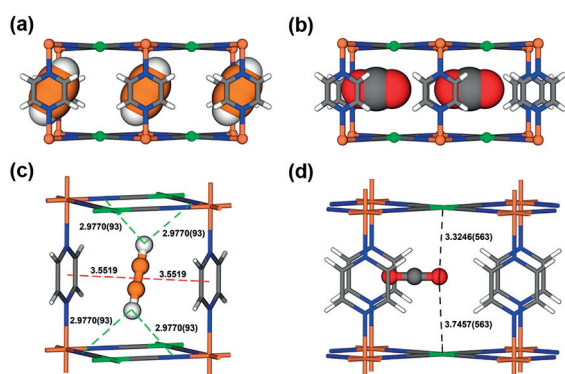


**Figure 4.** Neutron diffraction crystal structure of a)  $\text{FeNi-M'MOF} \supset \text{C}_2\text{D}_2$  and b)  $\text{FeNi-M'MOF} \supset \text{CO}_2$ , viewed from the  $a/b$  axis. Adsorption binding sites of c)  $\text{C}_2\text{D}_2$  and c)  $\text{CO}_2$  for  $\text{FeNi-M'MOF}$ . Fe, Ni, C, N, O, H in  $\text{FeNi-M'MOF}$  and  $\text{CO}_2$  are represented by orange, green, gray, blue, red, and white, respectively; C and D in  $\text{C}_2\text{D}_2$  are represented by orange and white, respectively. The labelled distance is measured in Å.

for favorable  $\text{Ni}^{\delta+} \cdots \text{O}^{\delta-} = \text{C} = \text{O}^{\delta-} \cdots \text{Ni}^{\delta+}$  interactions to form in the structure. Thus,  $\text{CO}_2$  molecules were adsorbed near the center of the channel and parallel to the channel.  $\text{O}^{\delta-}$  atom of  $\text{CO}_2$  inserts between the adjacent two  $\text{Ni}^{\delta+}$  atoms from different layers and the distance of  $\text{O}^{\delta-} \cdots \text{Ni}^{\delta+}$  are 3.746 and 3.325 Å, respectively (Figure 4d). This type interaction is relatively weak, consistent with the gentle adsorption isotherm and low  $Q_{\text{st}}$  value of  $\text{CO}_2$  in  $\text{FeNi-M'MOF}$ . The multiple binding sites of  $\text{FeNi-M'MOF}$  for gas molecules and its different binding modes toward  $\text{C}_2\text{H}_2$  and  $\text{CO}_2$  enable  $\text{FeNi-M'MOF}$  to selectively adsorb  $\text{C}_2\text{H}_2$  from  $\text{CO}_2$  with both high  $\text{C}_2\text{H}_2$  uptake and remarkable  $\text{C}_2\text{H}_2/\text{CO}_2$  selectivity.

In summary, highly selective  $\text{C}_2\text{H}_2/\text{CO}_2$  separation has been successfully realized by a mixed iron/nickel MOF  $\text{FeNi-M'MOF}$  using a metalloligand approach. The structural features of cyanonickelate and optimal pore channels in this MOF allow  $\text{C}_2\text{H}_2$  molecules to interact at multiple binding sites, with both very high  $\text{C}_2\text{H}_2$  uptake and  $\text{C}_2\text{H}_2/\text{CO}_2$  selectivity in volumetric ratio. The so-called dual functionality in this material enables this MOF to serve as one of the best materials for  $\text{C}_2\text{H}_2/\text{CO}_2$  separation in terms of  $\text{C}_2\text{H}_2$ -capture capability. This work also illustrates an outstanding example to further reveal the huge separation potential of MOF adsorbents, especially for challenging gas separation and purification. The active ongoing research affords tremendous opportunities for energy-efficient separation.

## Acknowledgements

This work was supported by the Zhejiang Provincial Natural Science Foundation of China (LY20E020001), National Natural Science Foundation of China (51602301 and 51672251), and the Welch Foundation (AX-1730). J.G. acknowledges the Fundamental Research Funds of Zhejiang Sci-Tech University (2019Q007).

## Conflict of interest

The authors declare no conflict of interest.

**Keywords:** acetylene · adsorption · gas separation · iron · metal-organic frameworks

**How to cite:** *Angew. Chem. Int. Ed.* **2020**, *59*, 4396–4400  
*Angew. Chem.* **2020**, *132*, 4426–4430

- [1] a) H. Li, L. Li, R.-B. Lin, W. Zhou, S. Xiang, B. Chen, Z. Zhang, *EnergyChem* **2019**, *1*, 100006; b) M. Ding, R. W. Flaig, H.-L. Jiang, O. M. Yaghi, *Chem. Soc. Rev.* **2019**, *48*, 2783–2828; c) R.-B. Lin, L. Li, H.-L. Zhou, H. Wu, C. He, S. Li, R. Krishna, J. Li, W. Zhou, B. Chen, *Nat. Mater.* **2018**, *17*, 1128–1133; d) M. K. Taylor, T. Runčevski, J. Oktawiec, J. E. Bachman, R. L. Siegelman, H. Jiang, J. A. Mason, J. D. Tarver, J. R. Long, *J. Am. Chem. Soc.* **2018**, *140*, 10324–10331; e) X. Cui, K. Chen, H. Xing, Q. Yang, R. Krishna, Z. Bao, H. Wu, W. Zhou, X. Dong, Y. Han, B. Li, Q. Ren, M. J. Zaworotko, B. Chen, *Science* **2016**, *353*, 141–144; f) A. Cadiau, K. Adil, P. M. Bhatt, Y. Belmabkhout, M. Eddaoudi, *Science* **2016**, *353*, 137–140; g) R.-B. Lin, S. Xiang, W. Zhou, B. Chen, *Chem* **2019**, <https://doi.org/10.1016/j.chempr.2019.1010.1012>.
- [2] a) K.-J. Chen, D. G. Madden, S. Mukherjee, T. Pham, K. A. Forrest, A. Kumar, B. Space, J. Kong, Q.-Y. Zhang, M. J. Zaworotko, *Science* **2019**, *366*, 241–246; b) Y. Liu, Z. Chen, G. Liu, Y. Belmabkhout, K. Adil, M. Eddaoudi, W. Koros, *Adv. Mater.* **2019**, *31*, 1807513; c) W. G. Cui, T. L. Hu, X. H. Bu, *Adv. Mater.* **2019**, *31*, 1806445; d) R. L. Siegelman, P. J. Milner, E. J. Kim, S. C. Weston, J. R. Long, *Energy Environ. Sci.* **2019**, *12*, 2161–2173; e) L. Li, R.-B. Lin, R. Krishna, H. Li, S. Xiang, H. Wu, J. Li, W. Zhou, B. Chen, *Science* **2018**, *362*, 443–446; f) P.-Q. Liao, N.-Y. Huang, W.-X. Zhang, J.-P. Zhang, X.-M. Chen, *Science* **2017**, *356*, 1193–1196; g) S. Yang, A. J. Ramirez-Cuesta, R. Newby, V. Garcia-Sakai, P. Manuel, S. K. Callear, S. I. Campbell, C. C. Tang, M. Schröder, *Nat. Chem.* **2014**, *7*, 121–129; h) M. L. Aubrey, M. T. Kapelewski, J. F. Melville, J. Oktawiec, D. Presti, L. Gagliardi, J. R. Long, *J. Am. Chem. Soc.* **2019**, *141*, 5005–5013.
- [3] C. R. Reid, K. M. Thomas, *J. Phys. Chem. B* **2001**, *105*, 10619–10629.
- [4] a) H. Yang, T. X. Trieu, X. Zhao, Y. Wang, Y. Wang, P. Feng, X. Bu, *Angew. Chem. Int. Ed.* **2019**, *58*, 11757–11762; *Angew. Chem.* **2019**, *131*, 11883–11888; b) J. Lee, C. Y. Chuah, J. Kim, Y. Kim, N. Ko, Y. Seo, K. Kim, T. H. Bae, E. Lee, *Angew. Chem. Int. Ed.* **2018**, *57*, 7869–7873; *Angew. Chem.* **2018**, *130*, 7995–7999; c) R.-B. Lin, L. Li, H. Wu, H. Arman, B. Li, R.-G. Lin, W. Zhou, B. Chen, *J. Am. Chem. Soc.* **2017**, *139*, 8022–8028; d) M. Jiang, X. Cui, L. Yang, Q. Yang, Z. Zhang, Y. Yang, H. Xing, *Chem. Eng. J.* **2018**, *352*, 803–810; e) H. S. Scott, M. Shivanna, A. Bajpai, D. G. Madden, K.-J. Chen, T. Pham, K. A. Forrest, A. Hogan, B. Space, J. J. Perry IV, M. J. Zaworotko, *ACS Appl. Mater. Interfaces* **2017**, *9*, 33395–33400; f) K.-J. Chen, H. S. Scott, D. G. Madden, T. Pham, A. Kumar, A. Bajpai, M. Lusi, K. A. Forrest, B. Space, J. J. Perry IV, M. J. Zaworotko, *Chem* **2016**, *1*, 753–765; g) O. T. Qazvini, R. Babarao, Z.-L. Shi, Y.-B. Zhang, S. G. Telfer, *J. Am. Chem. Soc.* **2019**, *141*, 5014–5020.
- [5] a) H. Zeng, M. Xie, Y.-L. Huang, Y. Zhao, X.-J. Xie, J.-P. Bai, M.-Y. Wan, R. Krishna, W. Lu, D. Li, *Angew. Chem. Int. Ed.* **2019**, *58*, 8515–8519; *Angew. Chem.* **2019**, *131*, 8603–8607; b) J. Duan, M. Higuchi, J. Zheng, S.-I. Noro, I.-Y. Chang, K. Hyeon-Deuk, S. Mathew, S. Kusaka, E. Sivaniah, R. Matsuda, *J. Am. Chem. Soc.* **2017**, *139*, 11576–11583; c) F. Luo, C. Yan, L. Dang, R. Krishna, W. Zhou, H. Wu, X. Dong, Y. Han, T.-L. Hu, M. O'Keefe, L.

- Wang, M. Luo, R.-B. Lin, B. Chen, *J. Am. Chem. Soc.* **2016**, *138*, 5678–5684.
- [6] a) Y.-L. Peng, T. Pham, P. Li, T. Wang, Y. Chen, K.-J. Chen, K. A. Forrest, B. Space, P. Cheng, M. J. Zaworotko, Z. Zhang, *Angew. Chem. Int. Ed.* **2018**, *57*, 10971–10975; *Angew. Chem.* **2018**, *130*, 11137–11141; b) Y.-P. Li, Y. Wang, Y.-Y. Xue, H.-P. Li, Q.-G. Zhai, S.-N. Li, Y.-C. Jiang, M.-C. Hu, X. Bu, *Angew. Chem. Int. Ed.* **2019**, *58*, 13590–13595; *Angew. Chem.* **2019**, *131*, 13724–13729; c) Y. Ye, Z. Ma, R.-B. Lin, R. Krishna, W. Zhou, Q. Lin, Z. Zhang, S. Xiang, B. Chen, *J. Am. Chem. Soc.* **2019**, *141*, 4130–4136.
- [7] a) D. Aguilà, Y. Prado, E. S. Koumoussi, C. Mathoniere, R. Clérac, *Chem. Soc. Rev.* **2016**, *45*, 203–224; b) M. B. Zakaria, T. Chikyow, *Coord. Chem. Rev.* **2017**, *352*, 328–345; c) K. Otsubo, T. Haraguchi, H. Kitagawa, *Coord. Chem. Rev.* **2017**, *346*, 123–138; d) S. Sakaida, K. Otsubo, O. Sakata, C. Song, A. Fujiwara, M. Takata, H. Kitagawa, *Nat. Chem.* **2016**, *8*, 377–383; e) M. M. Deshmukh, M. Ohba, S. Kitagawa, S. Sakaki, *J. Am. Chem. Soc.* **2013**, *135*, 4840–4849; f) J. T. Culp, M. R. Smith, E. Bittner, B. Bockrath, *J. Am. Chem. Soc.* **2008**, *130*, 12427–12434.
- [8] a) M. C. Das, S. Xiang, Z. Zhang, B. Chen, *Angew. Chem. Int. Ed.* **2011**, *50*, 10510–10520; *Angew. Chem.* **2011**, *123*, 10696–10707; b) S.-C. Xiang, Z. Zhang, C.-G. Zhao, K. Hong, X. Zhao, D.-R. Ding, M.-H. Xie, C.-D. Wu, M. C. Das, R. Gill, K. Tomas, B. Chen, *Nat. Commun.* **2011**, *2*, 204.
- [9] V. Niel, J. M. Martinez-Agudo, M. C. Muñoz, A. B. Gaspar, J. A. Real, *Inorg. Chem.* **2001**, *40*, 3838–3839.
- [10] J. Gao, J. Cong, Y. Wu, L. Sun, J. Yao, B. Chen, *ACS Appl. Energy Mater.* **2018**, *1*, 5140–5144.
- [11] X. Duan, Q. Zhang, J. Cai, Y. Yang, Y. Cui, Y. He, C. Wu, R. Krishna, B. Chen, G. Qian, *J. Mater. Chem. A* **2014**, *2*, 2628–2633.
- [12] J. Duan, W. Jin, R. Krishna, *Inorg. Chem.* **2015**, *54*, 4279–4284.
- [13] S. Xiang, W. Zhou, Z. Zhang, M. A. Green, Y. Liu, B. Chen, *Angew. Chem. Int. Ed.* **2010**, *49*, 4615–4618; *Angew. Chem.* **2010**, *122*, 4719–4722.
- [14] P. Li, Y. He, Y. Zhao, L. Weng, H. Wang, R. Krishna, H. Wu, W. Zhou, M. O’Keeffe, Y. Han, B. Chen, *Angew. Chem. Int. Ed.* **2015**, *54*, 574–577; *Angew. Chem.* **2015**, *127*, 584–587.
- [15] Y. He, R. Krishna, B. Chen, *Energy Environ. Sci.* **2012**, *5*, 9107–9120.
- [16] E. D. Bloch, W. L. Queen, R. Krishna, J. M. Zadrozny, C. M. Brown, J. R. Long, *Science* **2012**, *335*, 1606–1610.

Manuscript received: January 7, 2020

Accepted manuscript online: January 13, 2020

Version of record online: January 30, 2020